Cross section measurement of the ^{144}Sm(α, n) ^{147}Gd reaction for studying the α-nucleus optical potential at astrophysical energies

Gy. Gyürky [1,*], P. Mohr [1], A. Angyal [1], Z. Halász [1], G. G. Kiss [1], Zs. Mátyus [1,2], T. N. Szegedi [1], T. Szücs [1], and Zs. Fülöp [1]

[1]*Institute for Nuclear Research (ATOMKI), H-4001 Debrecen, Hungary*
[2]*University of Debrecen, Doctoral School of Physics, Egyetem tér 1., H-4032 Debrecen, Hungary*

Background: Nuclear reactions involving α particles play an important role in various astrophysical processes such as the γ process of heavy element nucleosynthesis. The poorly known low-energy α-nucleus optical potential is a key parameter to estimate the rates of these reactions.

Purpose: The α-nucleus optical potential can be tested by measuring the cross section of α scattering as well as α-induced reactions. Low energy elastic α scattering on ^{144}Sm has recently been measured with high precision. The aim of the present work was to complement that work by measuring the (α, n) cross sections on ^{144}Sm at low energies. The experimental data shall be used to constrain the α-nucleus optical model potential. From this potential the ^{144}Sm(α, γ) ^{148}Gd reaction rate can be derived with reduced uncertainties.

Method: The ^{144}Sm(α, n) ^{147}Gd reaction was studied by bombarding Sm targets with α beams provided by the cyclotron accelerator of Atomki. The cross section was determined using the activation method. The γ radiation following the decay of the ^{147}Gd reaction product was measured with a high-purity germanium (HPGe) detector. The experimental data are analyzed within the statistical model.

Results: The cross section was measured in the α-energy range between 13 and 20 MeV in 1 MeV steps, i.e., from close above the (α, n) threshold. The results were compared with statistical model calculations using various approaches and parametrizations for the α-nucleus optical potential, and excellent agreement was obtained for two recent potentials. However, these potentials cannot reproduce literature data for the ^{144}Sm(α, γ) ^{148}Gd reaction with the same accuracy.

Conclusions: Constraints for the α-nucleus potential were derived from an analysis of the new ^{144}Sm(α, n) ^{147}Gd data and literature data for ^{144}Sm(α, γ) ^{148}Gd. These constraints enable a determination of the re-action rate of the ^{144}Sm(α, γ) ^{148}Gd reaction with significantly reduced uncertainties of less than a factor of 2.

I. INTRODUCTION

The building up of chemical elements by stars involves many different processes during the various stages of stellar evolution. The final episode of a massive star's life is the core-collapse supernova explosion, which is the site of several nucleosynthesis processes, for example the astrophysical γ process [1,2]. The γ process—which may also take place in thermonuclear supernovae [3]—is thought to be the main process responsible for the synthesis of the so-called p isotopes. These isotopes are those heavy, proton rich species—between ^{74}Se and ^{196}Hg—which are not produced by neutron capture reactions in the s [4] and r processes [5].

The γ process proceeds through γ-induced reactions in the high temperature environment of a supernova. The main reactions are the neutron emitting (γ, n) reactions which drive the material towards the proton rich isotopes. Charged particle emitting (γ, p) and (γ, α) reactions are, however, equally

important if one wants to estimate the elemental and isotopic abundances resulting from a γ-process event.

Owing to the high number of reactions that participate in a γ-process network involving mostly unstable nuclei, experimental data for the reaction cross sections are very scarce and the astrophysical models are mainly based on theoretical reaction rates obtained from calculated cross sections. It has been found that, in the case of reactions involving α particles, the cross sections are very sensitive on the choice of the α-nucleus optical model potential (AOMP) and on its parameters. At low, astrophysically important energies (deep below the Coulomb-barrier), differences of up to two orders of magnitude are found between the various calculations. Moreover, the comparison with the very limited available experimental data shows that typically the calculations using global AOMPs are not able to reproduce the measured cross sections with the required precision. This introduces a large uncertainty into the astrophysical γ-process models.

The poor knowledge of AOMP necessitates its extensive experimental investigation. Traditionally, it has been studied with elastic α-scattering experiments where the deviation from the Rutherford cross section carries information about

*gyurky@atomki.hu

the AOMP. However, in order to have large enough deviation, the experiments have to be carried out at relatively high energies, above the astrophysical energy range. Nevertheless, elastic scattering is still a useful tool, as will be discussed later in the paper in relation to ^{144}Sm.

The AOMP can also be studied by measuring the cross section of α-induced nuclear reactions. Owing to their direct relevance for the γ process, the radiative capture (α, γ) reactions were studied in recent years on several isotopes (for a list of reactions see, e.g., [6]). In the case of these reactions, however, the typically very low cross sections at astrophysical energies renders the measurements rather difficult.

The problem related to the extremely low cross sections of the (α, γ) reactions can be circumvented by measuring a reaction channel governed by the strong interaction. For example, (α, n) reactions, if they are energetically possible, can also provide information about the AOMP, and their cross sections are typically orders of magnitude larger than those of the radiative capture. Close above the neutron threshold the (α, n) cross sections are sensitive mostly to the AOMP, which can therefore be studied with these kind of reactions. For further details about the sensitivities on the various parameters see, e.g., [7].

The p isotope of Samarium, ^{144}Sm, plays a special role in the history of γ-process studies. This was the first isotope on which (α, γ) cross section measurement was carried out in relation to the γ process and the problem with the AOMP was identified [8]. A recent experiment has confirmed those results [9]. An elastic α-scattering experiment on ^{144}Sm was carried out very recently at α energies of 16, 18, and 20 MeV [10]. The AOMP models were tested with these scattering data and it was found that even at 16 MeV the deviation from the Rutherford cross section is not large enough to draw conclusions with high confidence.

The threshold of the ^{144}Sm$(\alpha, n)^{147}$Gd reaction is at 12.6 MeV in the laboratory system. Above this energy, the ^{144}Sm$(\alpha, n)^{147}$Gd reaction can provide information about the AOMP of ^{144}Sm. There is only one data set for this reaction cross section in the literature, by Denzler *et al.* [11], but at the lowest energies—near the threshold—there are only few data points which bear high uncertainties both on the cross section value and on the energy scale. Cumulative activation yields from another experiment by Archenti *et al.* [12] can be used to extract two further data points for the ^{144}Sm$(\alpha, n)^{147}$Gd reaction. But these data also have significant energy uncertainties of 1.5 MeV. All data from the literature are thus not suitable for a stringent test of AOMP models. The aim of the present work is therefore to measure the ^{144}Sm$(\alpha, n)^{147}$Gd cross section with high precision from the reaction threshold up to the energy range of the recent elastic scattering experiment. The present results provide independent information about the ^{144}Sm $+\alpha$ AOMP and complement the findings of the elastic scattering and radiative capture experiments.

II. EXPERIMENTAL PROCEDURE

The reaction product of the ^{144}Sm$(\alpha, n)^{147}$Gd reaction is radioactive, decaying with a half-life of 38.06 ± 0.12 h to

^{147}Eu [13]. The decay is followed by the emission of some high intensity γ radiation. This allows the cross section measurement to be carried out by the γ detection based activation technique [14], which was thus used in the present work. In the following subsections, the most important features of the experimental procedure are described.

A. Target preparation and characterization

The p isotopes of heavy elements have typically very low isotopic abundances, often below 1%. ^{144}Sm is an exception with its natural abundance as high as $3.07 \pm 0.07\%$ [15]. This fact, combined with the relatively large cross section of the (α, n) reaction channel allowed the application of natural isotopic abundance targets.

The targets were prepared by electron beam evaporation of natural isotopic composition samarium oxide (Sm_2O_3) onto 6 μm thick Al foils. First information about the target thickness was obtained by weighing. The weight of the Al foils were measured to 1 μg precision before and after the evaporation. Knowing the evaporated surface of 16 mm in diameter, the target thickness could be calculated from the weight difference.

Since the weight does not give information about the target composition and the stoichiometry (i.e., the Sm:O ratio) which may change during the evaporation, the areal density of the Sm atoms—as the important quantity for the cross section determination— was measured with Rutherford backscattering spectrometry (RBS). For the RBS measurement a 2.0 MeV α beam provided by the Tandetron accelerator of Atomki [16] was used. The scattered α particles were detected by a collimated ion-implanted Si detector mounted at a backward angle of $165°$ with respect to the beam direction. The collected spectra were analyzed using SIMNRA [17], a widely used computer code for simulating and evaluating - among others - RBS spectra. The thicknesses from the RBS measurement were used for the cross section analysis which were in agreement with the weighing data within 5% when the Sm:O ratios obtained from the RBS analysis were used for the weight measurements.

Altogether five targets were prepared and the Sm thicknesses were measured to be in the range of (0.5–1.0)$\cdot 10^{18}$ atoms/cm^2 with a precision of 5%. Each target was used one or two times in the subsequent cross section measurement campaign. Thicker targets were used for lower energies where the cross sections are lower.

B. Irradiations

For the ^{144}Sm$(\alpha, n)^{147}$Gd cross section measurements, the targets were irradiated by α-beams provided by the K20 cyclotron accelerator of Atomki [18]. The irradiation chamber was the same as in our previous works, see e.g. [19]. The whole chamber served as a Faraday cup, allowing the determination of the number of projectiles by charge integration. The He^{++} beam intensity was typically 1 e μA.

The length of the irradiation varied between 2 and 24 hours, longer irradiation was used at lower energies where the cross section is smaller. During the irradiation the

beam current was recorded in multichannel scaling mode with one minute resolution so that the fluctuations in the beam intensity could be taken into account in the activation analysis [14].

The cross section measurements were carried out in the energy range from 13 MeV (close above the threshold) up to 20 MeV with 1 MeV steps. The highest energy coincides with the highest energy of the recent elastic scattering experiment on ^{144}Sm [10].

With one exception, a single target was irradiated in a single activation run. In the case of the $E_\alpha = 20$ MeV irradiation, however, two targets were placed in the chamber, one behind the other, separated by a 10 μm thick Al energy degrader foil, similar to the procedure of a recent experiment described in [20]. The thickness of the degrader foil was measured with α energy loss to a precision of 5% which was used for the effective energy determination at the second target (see section II D).

C. Detection of the decay radiation

The decay of the ^{147}Gd reaction product is followed by the emission of many different energy γ-radiations from numerous cascade transitions. For the cross section determination, we have used the four most intense radiations with energies 229.2 keV (57.7% ± 3.7%), 370.0 keV (15.7% ± 0.9%), 396.0 keV (31.4% ± 1.9%) and 929.0 keV (18.4% ± 1.1%). In parentheses the relative intensities are given which were taken from the latest nuclear data compilation [13].

After the irradiation the targets were removed from the chamber and transported to the off-line counting setup. This setup consisted of a LEPS detector (Low Energy Photon Spectrometer, a thin crystal high-purity germanium detector optimal for the detection of low-energy γ-radiation) and a complete 4π lead shielding with copper and cadmium liners [21].

In order to measure low activities, the targets were placed in close geometry in front of the detector, at a distance of 1 cm from the crystal. In such a close geometry, the true coincidence summing effect makes it difficult to determine precisely the detection efficiency and the activity of the produced ^{147}Gd source. Therefore, the so-called two-distance technique was used [14]. The absolute efficiency of the detector was measured with calibrated radioactive sources at far geometry (in this case at 10 cm from the detector) where the summing effect is negligible. Then the decay of a high activity ^{147}Gd source was measured both in close and far geometries. Based on the two measurements, an efficiency conversion factor between the two geometries was obtained for all studied transitions, which was then used for the low activity samples that could be measured only in close geometry.

The length of the γ-counting was between 12 and 140 hours and the spectra were stored hourly in order to follow the decay of ^{147}Gd. As an example, Fig. 1 shows a γ-spectrum which was measured on a target irradiated with an α-beam of 16 MeV. The peaks corresponding to the transitions used for the cross section determination are marked.
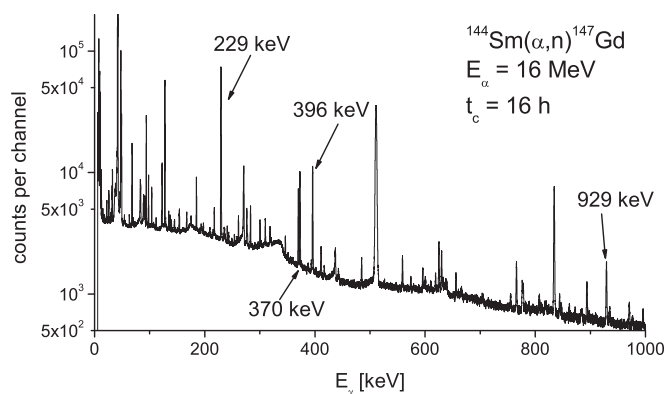

FIG. 1. Typical γ spectrum measured for 16 hours after irradiating the target with a 16 MeV α beam. The peaks corresponding to the transitions used for the cross section determination are marked. The channel width is about 0.1 keV.

D. Results

Table I shows the measured cross section values. The first column contains the primary α-beam energies provided by the cyclotron, while in the second column the effective interaction energies and their uncertainties are shown in the center-of-mass system. The effective energy calculation is based on the energy loss of the beam in the target layer. Since this energy loss is relatively small (a few tens of keV) and the cross section does not change much in such an energy interval, the effective energy was calculated for half of the target thickness. The uncertainty of the effective energy is made up by the uncertainty of the primary beam energy (0.3% from the energy calibration of the cyclotron), the target thickness, and the stopping power uncertainty. In the case of the measurement carried out with a degrader foil (marked with a footnote in the table), the energy uncertainty also includes the contribution of the degrader foil thickness.

The cross section results listed in the last column were calculated as the average of the values obtained from the four studied transitions, which were always in good agreement with each other. The uncertainty of the cross section is calculated as the quadratic sum of the following sources: target thickness (5%), detection efficiency including the far-close

TABLE I. Measured cross section of the ^{144}Sm$(\alpha, n)^{147}$Gd reaction.

E_{beam} (MeV)	$E_{\text{c.m.}}^{\text{eff}}$ (MeV)	Cross section (mbarn)
13.0	12.62 ± 0.04	0.139 ± 0.016
14.0	13.60 ± 0.04	1.36 ± 0.12
15.0	14.57 ± 0.05	8.03 ± 0.73
16.0	15.54 ± 0.05	31.0 ± 2.8
17.0	16.52 ± 0.05	98.3 ± 9.0
18.0	17.49 ± 0.06	188 ± 17
18.9[a]	18.33 ± 0.11	281 ± 25
20.0	19.43 ± 0.06	417 ± 36

[a]Measured with energy degrader foil.

geometry conversion factor (5%), beam current integration (3%), relative intensity of the ^{147}Gd decay radiation (5%), ^{144}Sm natural abundance (2.3%), and counting statistics ($<$5%).

III. THEORETICAL ANALYSIS

A. General remarks

It is the aim of the present study to provide further constraints for the calculation of α-induced cross sections on ^{144}Sm. These constraints will be based on the new ^{144}Sm(α, n) ^{147}Gd data from this work which will be complemented by further information from experiments on ^{144}Sm(α, γ) ^{148}Gd capture [8,9] and ^{144}Sm(α, α) ^{144}Sm elastic scattering [10,22].

The calculations are based on the statistical model approach. The following calculations were made with the widely used computer code TALYS [23]. In a schematic notation, the cross section of an (α, X) reaction is given by

$$\sigma(\alpha, X) \sim \frac{T_{\alpha,0} T_X}{\sum_i T_i} = T_{\alpha,0} \times b_X, \qquad (1)$$

with the transmission coefficients T_i into the i-th open channel and the branching ratio $b_X = T_X / \sum_i T_i$ for the decay into the channel X. Details of the formalism are given, e.g., in [7].

The T_i are calculated from global optical potentials for the particle channels and from the γ-ray strength function (GSF) for the photon channel. Besides the explicit dependence of the T_i on the optical potentials and the GSF, the T_i implicitly depend on the nuclear level densities (LDs) of the respective residual nuclei because each T_i is composed of the sum over few low-lying states j below the excitation energy E_0^* in the respective residual nucleus plus an integral over the LD for excitation energies above E_0^*.

$T_{\alpha,0}$ represents the transmission in the entrance channel (with the target ^{144}Sm in the ground state). Thus, $T_{\alpha,0}$ depends only on the chosen α-nucleus optical model potential (AOMP), but is independent of the chosen LD and other parameters of the statistical model. $T_{\alpha,0}$ is the most important quantity in Eq. (1) because it defines the total reaction cross section, σ_{reac}, for $\alpha + {}^{144}$Sm.

From Eq. (1) several basic properties of the reactions under study can be deduced. This is also illustrated in the level scheme (Fig. 2) and in the decomposition of the total cross section, σ_{reac}, into the the different exit channels (Fig. 3).

In general, for heavy target nuclei and low energies, the transmission of the α particle, $T_{\alpha,0}$, in the entrance channel is much smaller than other T_X like T_γ or T_n. Thus, below the neutron threshold, $b_\gamma \approx 1$, and the (α, γ) cross section depends only on $T_{\alpha,0}$. Above the neutron threshold, $b_n \approx 1$, and the (α, n) cross section depends only on $T_{\alpha,0}$. As $T_{\alpha,0}$ depends only on the chosen AOMP, experimental data for (α, γ) cross sections below the neutron threshold and for (α, n) cross sections above the neutron threshold are appropriate to constrain the AOMP without ambiguities from other ingredients of the statistical model. The relevance of the different exit channels is shown in Fig. 3; here the Atomki-V2 potential [24,25] was used as AOMP. Further discussion of the AOMP will be given later.
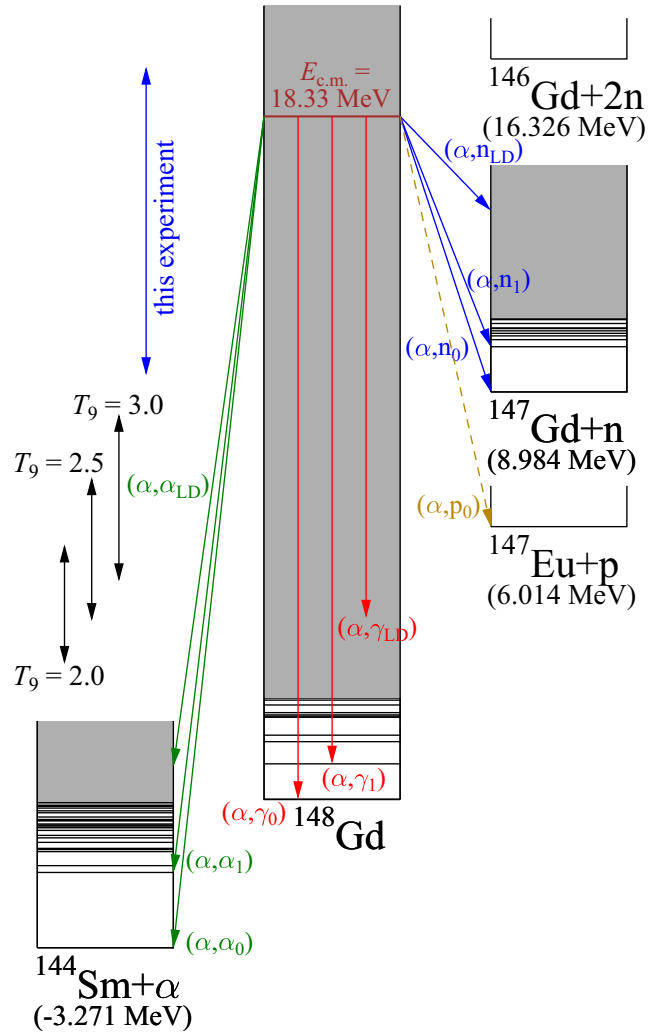

FIG. 2. Level scheme of ^{148}Gd: The ^{144}Sm(α, α) ^{144}Sm, ^{144}Sm(α, γ) ^{148}Gd, ^{144}Sm(α, p) ^{147}Eu, ^{144}Sm(α, n) ^{147}Gd, and ^{144}Sm$(\alpha, 2n)$ ^{146}Gd reactions are illustrated. For each of the residual nuclei (^{144}Sm, ^{148}Gd, ^{147}Eu, ^{147}Gd, ^{146}Gd), the low-lying levels below E_0^* are shown, which are used explicitly in the statistical model calculations. The grey-shaded areas above E_0^* are taken into account using the LD of the residual nuclei. As an example, the decay channels of the ^{148}Gd compound nucleus at $E_{\text{c.m.}} = 18.33$ MeV (corresponding to an excitation energy $E^* = 15.06$ MeV in ^{148}Gd) are shown. For each (α, X) channel, the (α, X_0) decay to the ground state, (α, X_1) decay to the first excited state, and one arrow for the (α, X_{LD}) decay to higher-lying states above E_0^* are shown; $(\alpha, X_{i \geqslant 2})$ decays are not shown for better readability. The vertical arrows indicate the standard Gamow window of the (α, γ) reaction for typical temperatures of $T = 2$–3 GK ($T_9 = 2$–3). For further discussion see text.

The above Eq. (1) is valid for laboratory experiments where the target nucleus is in its ground state. Thus, the transmission in the entrance channel is given by $T_{\alpha,0}$. In contrast, the high temperatures in the stellar interior lead to thermal population of excited states in the target nucleus. As a consequence, under stellar conditions Eq. (1) has to be extended to take into account that excited states in the target nucleus are
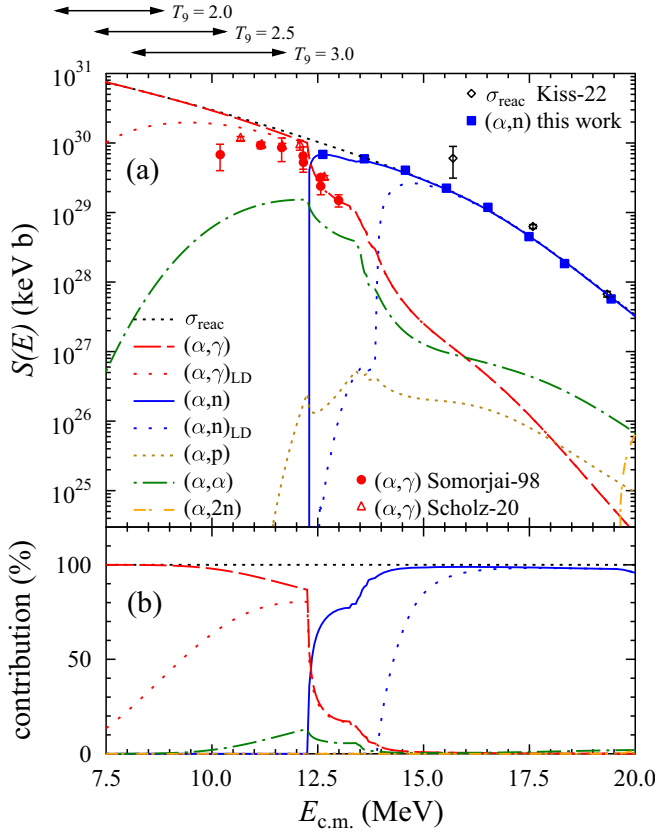
FIG. 3. Decomposition of the total reaction cross section, σ_{reac}, into the different (α, X) exit channels. All cross sections have been converted to astrophysical S factors in the upper part a); the lower part b) shows the contributions of the different reaction channels to the total reaction cross section, σ_{reac}, in a linear scale. $(\alpha, X)_{\text{LD}}$ shows the contribution of the higher-lying states above E_0^* for the two dominating (α, X) channels which are the (α, γ) and the (α, n) channel. The experimental data points represent total cross sections from (α, α) elastic scattering (black open diamonds, [10]), (α, n) cross sections from this work (blue full squares), and (α, γ) cross sections (red full circles [8] and red open triangles [9]). The arrows indicate the standard Gamow window for typical temperatures of $T_9 = 2 - 3$. For further discussion see text.

thermally populated, leading to an entrance channel transmission T_α instead of $T_{\alpha,0}$. But the transmissions $T_{\alpha,i>0}$ to excited states of the target nucleus are typically smaller than $T_{\alpha,0}$ to the ground state. Thus, T_α remains smaller than T_γ or T_n under typical stellar conditions because the Coulomb barrier suppresses transitions to excited states. Hence, stellar cross sections and the resulting stellar reaction rates of α-induced reactions depend mainly on the chosen AOMP.

Furthermore, because $T_{\alpha,0}$ is the dominating contributor to the total α transmission, T_α, the stellar reaction rate, $N_A \langle \sigma v \rangle^*$, of the (α, γ) reaction remains close to the laboratory rate, $N_A \langle \sigma v \rangle_{\text{lab}}$, which is calculated from the (α, γ) cross section under laboratory conditions (i.e., with ^{144}Sm in its 0^+ ground state). In contrast, excited states in ^{148}Gd play an essential role in the stellar $N_A \langle \sigma v \rangle^*$. Consequently, (α, γ) experiments in the laboratory are well-suited to determine

the stellar (α, γ) rate. The stellar (γ, α) rate is then derived from the stellar (α, γ) rate using the formalism of detailed balance. For completeness we note that (γ, α) experiments cannot provide the stellar (γ, α) rate because of the missing contributions of thermally excited states in the target nucleus.

B. Relevance of different exit channels and sensitivities

A detailed investigation of Fig. 3 provides an excellent intuitive way to understand the sensitivities on the chosen parameters for the statistical model. It is obvious from Fig. 3 that there are two dominating channels: the (α, γ) channel below the (α, n) threshold at 12.255 MeV, and the (α, n) channel above the (α, n) threshold. Compound-elastic and compound-inelastic scattering reach a maximum contribution of about 15%, close below the (α, n) threshold, but remain very marginal for most energies (e.g., far less than 10% below 10 MeV and above 13 MeV). The $(\alpha, 2n)$ channel opens above the experimental energy range of this work at 19.6 MeV. Although the $(\alpha, 2n)$ contribution increases steeply with energy, it remains below a few percent up to 20 MeV in Fig. 3. The contribution of the (α, p) channel remains far below 1% in the energy range of Fig. 3. This leads to the following approximate simplifications of Eq. (1):

(α, γ) cross section below the (α, n) threshold:

$$\sigma(\alpha, \gamma) \sim T_{\alpha,0} \times \frac{T_\gamma}{T_\gamma + T_\alpha} \tag{2}$$

$$\approx T_{\alpha,0} \quad \text{for } E \lesssim 10 \text{ MeV.} \tag{3}$$

(α, γ) cross section above the (α, n) threshold:

$$\sigma(\alpha, \gamma) \sim T_{\alpha,0} \times \frac{T_\gamma}{T_\gamma + T_\alpha + T_n} \tag{4}$$

$$\approx T_{\alpha,0} \times \frac{T_\gamma}{T_n} \quad \text{for } E \gtrsim 13 \text{ MeV.} \tag{5}$$

(α, n) cross section above the (α, n) threshold:

$$\sigma(\alpha, n) \sim T_{\alpha,0} \times \frac{T_n}{T_\gamma + T_\alpha + T_n} \tag{6}$$

$$\approx T_{\alpha,0} \quad \text{for } E \gtrsim 13 \text{ MeV.} \tag{7}$$

All T_i (except $T_{\alpha,0}$ in the entrance channel) are composed of a sum over low-lying states and an integral over the level density in the respective residual nucleus. By default, TALYS considers the first ten low-lying excited states explicitly; the contributions of higher-lying excited states are calculated using a continuous distribution of levels from a level density formula. Thus, in principle all T_i in Eqs. (2)–(7) and the resulting (α, γ) and (α, n) cross sections depend implicitly on the chosen level density.

In practice, the dependence of the (α, γ) and (α, n) cross sections on the chosen level density remains marginal. In the case of the (α, n) cross section, the low-lying states dominate only from threshold up to about 14 MeV; above 15 MeV, the contribution of the higher-lying excited states, which is simulated by the level density, exceeds 80%. Any change in the level density affects whether the (α, n) cross section is dominated by low-lying excited states or by high-lying excited states, but does not affect the total (α, n) cross section (as

measured in the activation experiment). In the case of the
(α, γ) cross section, the contribution of high-lying states is
increasing with energy and exceeds 50% around 9 MeV; i.e.,
all available experimental data points of [8,9] are governed by
transitions to higher-lying excited states in ^{148}Gd. Neverthe-
less, a significant relevance of the level density appears only
above the (α, n) threshold; see also Eq. (5). Below the (α, n)
threshold, the (α, γ) cross section practically depends only on
$T_{\alpha,0}$ and thus on the AOMP; see Eq. (3).

Summarizing the above findings, the new (α, n) data can
be used to constrain the AOMP. The few available (α, γ) data
points above the (α, n) threshold provide some information on
the γ-ray strength function and the level density of ^{148}Gd, and
the (α, γ) data below the (α, n) threshold should be well pre-
dicted because these (α, γ) data depend only on the AOMP,
which is well-constrained by the (α, n) data. Consequently,
the following discussion focuses on the AOMP whereas the
other ingredients of the statistical model calculations are only
briefly mentioned. For completeness, we point out that the
(α, γ) reaction rate for typical γ process temperatures of
$T_9 = 2$–3 is defined by the (α, γ) cross section below the
(α, n) threshold, and thus the (α, γ) reaction rate also depends
only on the AOMP.

C. Comparison of experimental and theoretical (α, n) cross sections

Figure 4 compares the new experimental (α, n) data to the
predictions of various AOMPs. It is obvious from Fig. 4 that
the earlier data by Denzler *et al.* [11] and Archenti *et al.* [12]
are not suitable to constrain the AOMP. In both experiments,
the stacked-foil technique was used, which leads to consid-
erable uncertainties in the energy, in particular when using
degrader foils where uncertainties in target foils and degrader
foils sum up at the last targets. (Note that the lowest data point
by Archenti *et al.* at 13.1 MeV is not shown in Fig. 4 because
it is located about three orders of magnitude above the present
data and all calculations, and is thus far out of the scale of
Fig. 4.)

The widely used simple four-parameter AOMP by McFad-
den and Satchler [27] fits the new data at higher energies;
however, at lower energies close above the threshold this
AOMP clearly overestimates the experimental data. Such an
overestimation towards lower energies has been found also
for the ^{144}Sm(α, γ) ^{148}Gd reaction [8,9]. An explanation for
the overestimation of low-energy cross sections was provided
in [24], and is related to the tail of the imaginary potential at
large radii above 10 fm (far beyond the colliding nuclei).

The three versions of the AOMP by Demetriou *et al.* [28]
underestimate the new (α, n) data over the whole energy range
under study. The most elaborated version 3 of the Demetriou
potentials is closer to the experimental data than versions 1
and 2, which do not take into account the dispersive coupling
between the real and imaginary parts of the AOMP.

The Atomki-V2 AOMP [24] and the AOMP by Avrigeanu
et al. [26] reproduce all new (α, n) data points within their
small experimental uncertainties, which is a remarkable suc-
cess for both AOMPs. As a consequence, the new (α, n) data
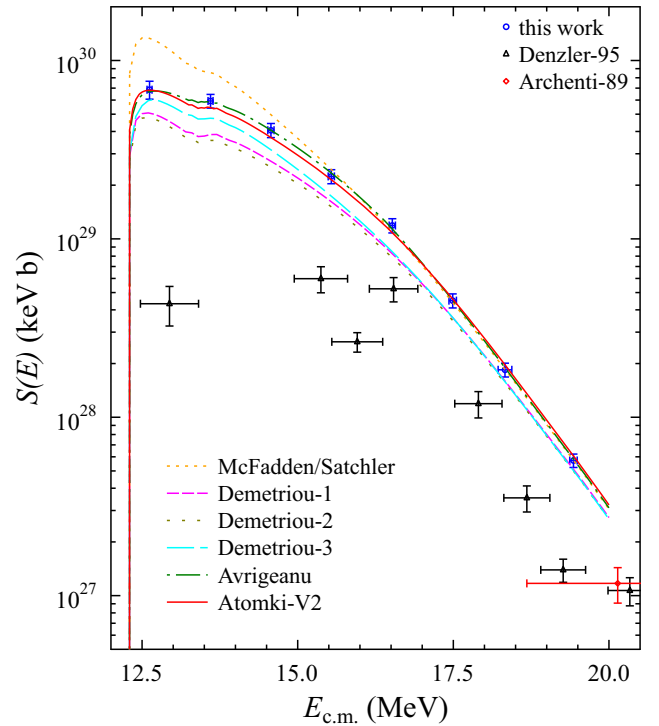support these two AOMPs, but cannot indicate a preferred

FIG. 4. Comparison of experimental ^{144}Sm(α, n) ^{147}Gd cross
section (shown as astrophysical S factor) to predictions from dif-
ferent AOMPs. Additional experimental data are taken from the
literature [11,12]; the lower data point of [12] at 13.1 MeV is about
three orders of magnitude above the present data (not shown). The
Atomki-V2 AOMP and the AOMP by Avrigeanu *et al.* [26] repro-
duce all new experimental data within their error bars. For further
discussion see text.

AOMP for the calculation of the ^{144}Sm(α, γ) ^{148}Gd reaction
rate.

It has been shown in earlier work (e.g., [6,29,30]) that three
further AOMPs which are available in TALYS, are not rec-
ommended for the calculation of low-energy cross sections.
These potentials by Watanabe [31], Nolte *et al.* [32], and
Avrigeanu *et al.* [33] are omitted in the present analysis.

D. Discussion of the various α-nucleus potentials

In this section we provide some basic information on the
various AOMPs under study in the present work which are the
AOMPs by McFadden and Satchler [27] (MCF), Demetriou
et al. [28] (third version of these AOMPs, DEM-3), Avrigeanu
et al. [26] (AVR), and the new Atomki-V2 AOMP [24].

The MCF AOMP was derived from elastic scattering at en-
ergies around 25 MeV. It is a very simple energy-independent
four-parameter AOMP. Because of its simplicity, the MCF
AOMP is widely used; e.g., the NON-SMOKER calculations of
reaction rates [34] utilize the MCF AOMP, and these rates are
adopted in the REACLIB database used in many astrophys-
ical models [35]. Whereas the MCF AOMP can be applied
successfully to low-energy data in the $A \approx 20$–50 mass range
[36], the MCF AOMP fails at sub-Coulomb energies in the

heavy mass range; see, e.g., [8,9] for the ^{144}Sm$(\alpha, \gamma)^{148}$Gd reaction and [6,37,38] for other target nuclei.

The DEM-3 AOMP has become the basis for α-induced reaction rates in the STARLIB database [39]. The DEM-3 AOMP is based on the double-folding approach and takes into account the dispersive coupling between the real and imaginary parts of the AOMP. Its parameters were adjusted to a limited set of low-energy reaction and scattering data which was available about 20 years ago. In particular, this data set includes the ^{144}Sm$(\alpha, \gamma)^{148}$Gd data of Somorjai *et al.* [8]. Because of the high astrophysical relevance, much effort was spent for the DEM-3 AOMP to fit the (α, γ) data point at the lowest energy, which shows an unexpectedly small cross section with a huge error bar. This attempt to fit the very small (α, γ) cross section may be one explanation for the underestimation of the (α, n) cross sections of the present work using the DEM-3 AOMP.

Similarly to the DEM-3 AOMP, the AVR AOMP is also based on the double-folding approach. However, at the end a Woods-Saxon parametrization was introduced [40], and the Woods-Saxon parameters were fine-tuned to a wider data set of reaction cross sections and elastic scattering angular distributions, finally leading to an energy-dependent many-parameter AOMP which was able to reproduce practically all available experimental data at that time. Because of this success, the AVR AOMP has been adopted as the default AOMP in TALYS for several years.

Similarly to the DEM-3 and AVR AOMPs, the Atomki-V2 AOMP is based on the double-folding approach. In contrast to the previous AOMPs, its parameters are obtained from a compilation of low-energy elastic scattering only [41]; no adjustment to reaction data was made. As it was noticed that usual optical model calculations become extremely sensitive to the tail of the imaginary potential at extreme sub-Coulomb energies, the Atomki-V2 AOMP uses a very narrow, deep, and sharp-edged imaginary part which avoids complications with the tail of the imaginary potential and leads to cross sections similar to a simple barrier transmission approach. It is interesting to note that this simple barrier transmission approach in combination with the energy-independent Atomki-V2 AOMP is able to predict reaction cross sections without any adjustment to reaction data; these predictions are for many targets surprisingly close to the energy-dependent multiparameter approach of the AVR AOMP. This holds also for the present study of the ^{144}Sm$(\alpha, n)^{147}$Gd reaction (see Fig. 4).

IV. ASTROPHYSICAL REACTION RATE OF THE ^{144}Sm$(\alpha, \gamma)^{148}$Gd REACTION

A. General remarks

The ^{144}Sm$(\alpha, \gamma)^{148}$Gd reaction has gained much attention in recent decades because its inverse ^{148}Gd$(\gamma, \alpha)^{144}$Sm reaction has strong a impact on the production ratio, $P_{146/144}$, for the two samarium isotopes ^{144}Sm and ^{146}Sm under γ process conditions. ^{144}Sm is a stable p nucleus which is directly produced by ^{148}Gd$(\gamma, \alpha)^{144}$Sm, whereas ^{146}Sm is an unstable α-emitter with a half-life of about 10^8 years which is produced
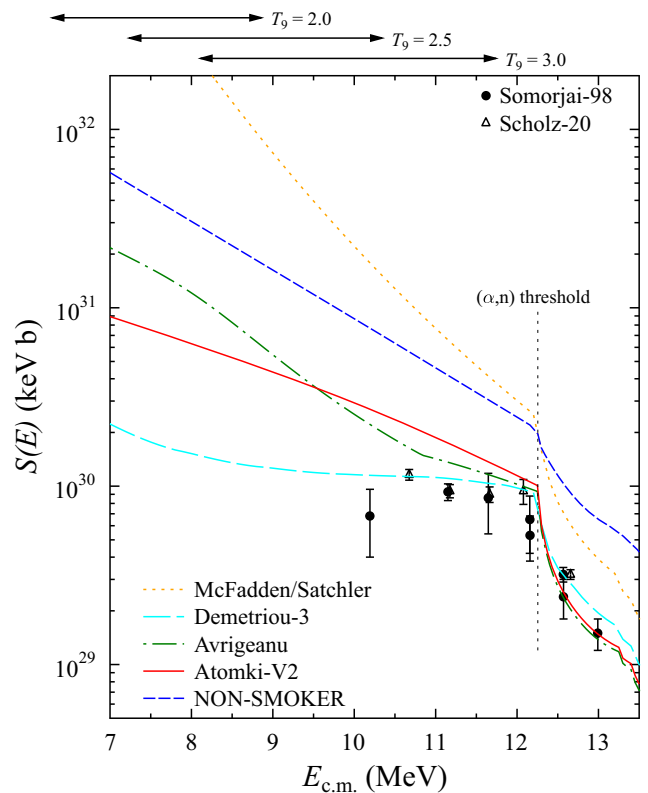

FIG. 5. Comparison of experimental ^{144}Sm$(\alpha, \gamma)^{148}$Gd cross section (shown as astrophysical S factor) to predictions from different AOMPs. The experimental data are taken from [8,9]. The thin vertical line indicates the (α, n) threshold. For energies below, the (α, γ) cross section depends practically only on the AOMP. The horizontal bars on top indicate the standard Gamow windows for typical temperatures of the γ process. For further discussion see text.

by ^{148}Gd$(\gamma, n)^{147}$Gd$(\gamma, n)^{146}$Gd and subsequent β decays to ^{146}Eu and ^{146}Sm. Nowadays, an excess of the ^{142}Nd / ^{144}Nd ratio is found in correlation with the samarium-to-neodymium ratio in meteoritic samples. This excess of ^{142}Nd reflects the α decay of ^{146}Sm and can be used as a cosmochronometer, provided that the initial production ratio, $P_{146/144}$, can be calculated reliably and the ratio at the formation of our solar system $P_{146/144} = 0.008\,40(32)$ [42] is well known; see, e.g., [2,42–46] and references therein, including the basic ideas in [47,48] and early measurements [49–52].

B. Comparison of experimental and theoretical (α, γ) cross sections

Figure 5 compares the experimental data of the ^{144}Sm$(\alpha, \gamma)^{148}$Gd reaction to the predictions of selected AOMPs (see previous Sec. III D). As the (α, γ) cross section below the (α, n) threshold depends practically only on the chosen AOMP, one should expect that the AVR and Atomki-V2 AOMPs are able to reproduce the experimental (α, γ) data because the AVR and Atomki-V2 AOMPs worked excellent for the (α, n) data (see Fig. 4). Somewhat surprisingly, this is not the case. The predictions from the AVR and Atomki-V2 AOMPs remain close to each other within about 20–30%

above 9 MeV. Only towards very low energies below 8 MeV does the AVR prediction exceed the Atomki-V2 prediction by more than a factor of 2.

Both the AVR and Atomki-V2 predictions are, however, a factor of about 1.5–2 above the low-energy data of [8,9]. In contrast, the DEM-3 AOMP fits the experimental (α, γ) data quite well, but was not able to fit the new (α, n) data. A simultaneous description of the (α, γ) and (α, n) data is not possible within the available AOMPs and would require introducing a very special energy dependence. However, such a special energy dependence may lead to significant uncertainties in the extrapolation towards energies below the lowest experimental (α, γ) data points. Such an extrapolation is necessary for the calculation of the astrophysical reaction rate $N_A\langle\sigma v\rangle$.

As expected, the MCF AOMP overestimates the experimental (α, γ) cross sections at all energies. This overestimation becomes most pronounced towards low energies. Somewhat surprisingly, the (α, γ) cross sections from the NON-SMOKER code [53] deviate significantly from the present calculation using the MCF AOMP. As also NON-SMOKER uses the MCF AOMP, this difference must result from different numerical treatments in the TALYS and NON-SMOKER codes.

C. Recommendations for the (α, γ) reaction rate

Taking into account the main result of the previous Sec. IV B that it is practically impossible to fit simultaneously the new (α, n) data and the literature (α, γ) data, it remains a difficult task to provide a reliable reaction rate, $N_A\langle\sigma v\rangle$, of the ^{144}Sm$(\alpha, \gamma)^{148}$Gd reaction. Despite these problems, significant progress is achieved when compared to the widely used conclusion that (α, γ) rates are uncertain by at least a factor of 10 (see, e.g., [54]).

We have calculated the astrophysical reaction rate, $N_A\langle\sigma v\rangle$, for the different AOMPs under study. The results are shown in Fig. 6. For the interpretation of the (α, γ) cross sections in Fig. 5 and the reaction rates, $N_A\langle\sigma v\rangle$, in Fig. 6 it is important to note that the classical Gamow windows (as, e.g., indicated by the horizontal arrows on top of Fig. 5) are calculated under the assumption of a constant (energy-independent) astrophysical S factor. However, for heavy nuclei the S factor typically has a noticeable negative slope, leading to a shift of the real Gamow window towards lower energies by about 1 MeV [55]. Because the reaction rate, $N_A\langle\sigma v\rangle$, in the upper part of Fig. 6 is an extremely temperature-dependent quantity, for better comparison the lower part of Fig. 6 shows the ratio of the respective rates to the rate from the Atomki-V2 AOMP.

It was shown in [24] that the predictions from the Atomki-V2 AOMP typically match experimental data with deviations below a factor of 2 for a wide range of heavy target nuclei. Consequently, astrophysical reaction rates from the Atomki-V2 AOMP should be well defined within an uncertainty factor of 2. This assumed uncertainty is indicated by the grey-shaded error band in Fig. 6.

Because of the close similarity of the calculated (α, γ) cross sections from the Atomki-V2 and AVR AOMPs, the
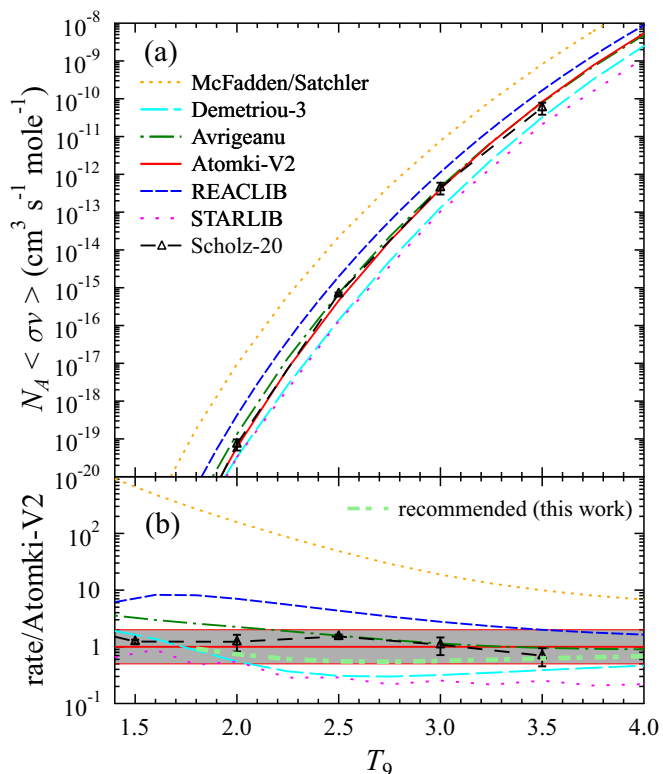

FIG. 6. Astrophysical reaction rate, $N_A\langle\sigma v\rangle$, from different AOMPs [upper part (a)] and ratio to the rate from the Atomki-V2 AOMP [lower part (b)]. The gray-shaded band shows the expected uncertainty of a factor of 2 from the Atomki-V2 AOMP [24]. For further discussion see text.

rate from the AVR AOMP remains well within the estimated uncertainty band from the Atomki-V2 AOMP for typical temperatures of the γ process of about $T_9 = 2$–3. Only towards lower temperatures does the rate from the AVR AOMP clearly exceed the rate from the Atomki-V2 AOMP; this excess corresponds to the steeply increasing S factor of the AVR AOMP towards lower energies. Around 7 MeV the cross section from the AVR AOMP is higher by a factor of 2 than the Atomki-V2 cross section, leading to an enhanced rate by a factor of 2 at $T_9 \approx 2$.

The rate from the DEM-3 AOMP is lower by about a factor of 2–3 in the temperature range of the γ process. However, at very low temperatures below $T_9 \approx 1.7$ the rate from the DEM-3 AOMP exceeds the Atomki-V2 rate; this results from a steep increase of the astrophysical S factor for the DEM-3 AOMP at energies below the shown range of Fig. 5. The STARLIB rate which is based on the DEM-3 AOMP is close to the present calculation of the DEM-3 AOMP. The minor differences may arise from the earlier TALYS version used for the STARLIB rates and from the enhanced accuracy settings in the present rate calculation.

The REACLIB rate is based on the NON-SMOKER calculation of the (α, γ) cross section using the MCF AOMP (see also Fig. 5 and discussion above). As this cross section does not agree with the present calculation using the MCF AOMP,

it is not recommended to use the REACLIB rate for the ^{144}Sm(α, γ) ^{148}Gd reaction.

The rate by Scholz *et al.* is based on a hyperparameter optimization of TALYS calculations which were adjusted to the available experimental ^{144}Sm(α, γ) ^{148}Gd data [8,9]. This rate is remarkably close to the rates from the Atomki-V2 and AVR AOMPs.

Before a final recommendation of the ^{144}Sm(α, γ) ^{148}Gd rate can be given, the apparent tension between the lowest experimental (α, γ) data points by Somorjai *et al.* [8] and Scholz *et al.* [9] (see also Fig. 5) needs further investigation. For shorter notation, all S factors in the following paragraphs are given in units of 10^{30} keV b.

Somorjai *et al.* report an S factor of 0.713(292) at $E = 10.193$ MeV. Using an updated half-life of ^{148}Gd, Scholz *et al.* correct that value to 0.68(28). For a consistent comparison of the two activation data sets, the same half-life of ^{148}Gd has to be used; thus, the latter value is taken for comparison here. Scholz *et al.* report their lowest S factor of 1.16(8) at $E = 10.675$ MeV.

For a comparison at $E = 10.193$ MeV, the S factor by Scholz *et al.* at 10.675 MeV has to be extrapolated down to $E = 10.193$ MeV. For this purpose, the theoretical energy dependence from the recent AOMPs was used. The ratio between the S factors at 10.193 MeV and 10.675 MeV is 1.03 (1.35, 1.24) from the DEM-3 (AVR, Atomki-V2) AOMPs; the average ratio is 1.21. This number changes only marginally to 1.26 if further AOMPs (DEM-1, DEM-2, MCF) are considered. This leads to an extrapolated S factor at 10.193 MeV of 1.40 and an interval between 1.20 and 1.57 from the lowest and highest theoretical ratios. Thus, the extrapolation procedure leads to an additional uncertainty of about 14% for the S factor at 10.193 MeV which has to be added to the 7% uncertainty of the original data point of Scholz *et al.*

The S factor and uncertainty of 0.68(28) of Somorjai *et al.* at 10.193 MeV may be slightly misleading; this becomes obvious from the resulting 3σ interval from -0.16 to 1.52 with its nonphysical negative lower limit. Relatively large uncertainties should be provided as an uncertainty factor of the underlying log-normal distribution. A careful estimate from the lower 1σ interval leads to an uncertainty factor of $\frac{0.68}{0.68-0.28} = 1.70$ for the lowest data point of Somorjai *et al.* Using this uncertainty factor of 1.70 for a realistic estimate of the upper end of the 1σ interval leads to an upper S factor of 1.16 which is quite close to the lower 1σ limit of the extrapolated data point by Scholz *et al.* (as derived in the previous paragraph). Consequently, the apparent tension between the lowest data points of Somorjai *et al.* and Scholz *et al.* is not very significant and results mainly from the misunderstandable linear specification of the uncertainties by Somorjai *et al.*

This leads us finally to the following recommendation for the ^{144}Sm(α, γ) ^{148}Gd reaction rate. The rate from the Atomki-V2 AOMP should be considered as an upper limit because Atomki-V2 fits the (α, n) data very well, but overestimates the (α, γ) data at low energies. Contrary, the DEM-3 AOMP fits the (α, γ) data well, but systematically underestimates the (α, n) data. Thus, the rate from the DEM-3 AOMP

TABLE II. Recommended reaction rate, $N_A\langle\sigma v\rangle$, and lower and upper limits for the ^{144}Sm(α, γ) ^{148}Gd reaction. All rates are given in units of cm^{3}s^{-1}mol^{-1}.

T_9	Lower limit	Upper limit	Recommended
2.00	3.29×10^{-20}	5.97×10^{-20}	4.43×10^{-20}
2.25	2.68×10^{-18}	7.27×10^{-18}	4.42×10^{-18}
2.50	1.39×10^{-16}	4.55×10^{-16}	2.52×10^{-16}
2.75	5.06×10^{-15}	1.69×10^{-14}	9.26×10^{-15}
3.00	1.31×10^{-13}	4.11×10^{-13}	2.32×10^{-13}
3.50	3.23×10^{-11}	8.36×10^{-11}	5.20×10^{-11}
4.00	2.51×10^{-09}	5.40×10^{-09}	3.68×10^{-09}

can be considered as a lower limit of the rate. This consideration is further strengthened by the relatively small slope of the astrophysical S factor from the DEM-3 AOMP towards lower energies down to about 7 MeV. The disagreement between the DEM-3 S factor and the lowest experimental data point by Somorjai *et al.* is not very significant because of the large uncertainty of this data point (see discussion in the previous paragraphs). The recommended rate is then derived from the geometric mean of the lower and upper limits of the rate. The results are listed in Table II.

It is important to point out that the upper and lower limits of the rate do not deviate by more than a factor of 3–4 over the whole relevant temperature range of $T_9 = 2$–3. Thus, the recommended rate does not deviate by more than a factor of 2 from the Atomki-V2 rate and the DEM-3 rate. A slightly larger deviation of a factor of about 3 is found between the recommended rate and the rates from the AVR AOMP and from the hyperparameter optimization in [9]. Compared to earlier conclusions that the reaction rates of α-induced reactions are very uncertain by at least a factor of 10, the situation has improved significantly for the ^{144}Sm(α, γ) ^{148}Gd reaction by a major reduction of the uncertainty.

V. SUMMARY AND CONCLUSIONS

The ^{144}Sm(α, n) ^{147}Gd reaction was studied at energies from the (α, n) threshold up to about 20 MeV. The new experimental data have significantly smaller uncertainties than the few available data in the literature [11,12]. Thus, the data can be used to constrain the α-nucleus optical model potential because a sensitivity study shows that the new (α, n) data are almost exclusively sensitive to the chosen AOMP.

It is found that the new experimental data can be described very well using the Atomki-V2 and AVR AOMPs. However, it turns out that these two AOMPs slightly overestimate the existing data for ^{144}Sm(α, γ) ^{148}Gd [8,9]. This is a somewhat surprising result as the (α, γ) data are also sensitive only to the chosen AOMP. In contrast, the DEM-3 AOMP fits the (α, γ) data better, but clearly underestimates the new (α, n) data.

As a consequence, our final recommended rate has to result from a compromise between the lower rate from the DEM-3 AOMP and the higher rates from the Atomki-V2 and AVR AOMPs. On the one hand, this is not a fully satisfying situa-

ation because of the tension in the reproduction of the new (α, n) data and the (α, γ) data from the literature, which calls for further investigations. On the other hand, the uncertainty of the recommended rate is now much smaller when compared to earlier estimates of a factor of 10 or more. The achieved accuracy of the ^{144}Sm(α, γ)^{148}Gd rate in combination with the overall improvement for α-induced reaction rates [25] should now permit stronger constraints for astrophysical conclusions for the γ process, similar to what has already been achieved very recently for the weak r process [56].

[1] M. Arnould and S. Goriely, Phys. Rep. **384**, 1 (2003).

[2] T. Rauscher, N. Dauphas, I. Dillmann, C. Fröhlich, Z. Fülöp, and G. Gyürky, Rep. Prog. Phys. **76**, 066201 (2013).

[3] C. Travaglio, F. K. Röpke, R. Gallino, and W. Hillebrandt, Astrophys. J. **739**, 93 (2011).

[4] F. Käppeler, R. Gallino, S. Bisterzo, and W. Aoki, Rev. Mod. Phys. **83**, 157 (2011).

[5] J. J. Cowan, C. Sneden, J. E. Lawler, A. Aprahamian, M. Wiescher, K. Langanke, G. Martínez-Pinedo, and F.-K. Thielemann, Rev. Mod. Phys. **93**, 015002 (2021).

[6] T. Szücs, P. Mohr, G. Gyürky, Z. Halász, R. Huszánk, G. G. Kiss, T. N. Szegedi, Z. Török, and Z. Fülöp, Phys. Rev. C **100**, 065803 (2019).

[7] T. Rauscher, Int. J. Mod. Phys. E **20**, 1071 (2011),.

[8] E. Somorjai, Z. Fülöp, A. Z. Kiss, C. E. Rolfs, H. P. Trautvetter, U. Greife, M. Junker, S. Goriely, M. Arnould, M. Rayet, T. Rauscher, and H. Oberhummer, Astron. Astrophys. **333**, 1112 (1998).

[9] P. Scholz, H. Wilsenach, H. W. Becker, A. Blazhev, F. Heim, V. Foteinou, U. Giesen, C. Münker, D. Rogalla, P. Sprung, A. Zilges, and K. Zuber, Phys. Rev. C **102**, 045811 (2020).

[10] G. G. Kiss, P. Mohr, G. Gyürky, T. Szücs, L. Csedreki, Z. Halász, Z. Fülöp, and E. Somorjai, Phys. Rev. C **106**, 015802 (2022).

[11] F.-O. Denzler, F. Rösch, and S. M. Qaim, Radiochimica Acta **69**, 209 (1995).

[12] A. Archenti, M. J. Ozafran, and S. J. Nassiff, J. Radioanal. Nucl. Chem. **132**, 139 (1989).

[13] N. Nica, Nucl. Data Sheets **110**, 749 (2009).

[14] Gy. Gyürky, Zs. Fülöp, F. Käppeler, G. G. Kiss, and A. Wallner, Eur. Phys. J. A **55**, 41 (2019).

[15] K. J. R. Rosman and P. D. P. Taylor, Pure Appl. Chem. **70**, 217 (1998).

[16] I. Rajta, I. Vajda, Gy. Gyürky, L. Csedreki, A. Kiss, S. Biri, H. van Oosterhout, N. Podaru, and D. Mous, Nucl. Instrum. Methods Phys. Res., Sect. A **880**, 125 (2018).

[17] M. Mayer, SIMNRA version 6.06

[18] S. Biri, I. K. Vajda, P. Hajdu, R. Rácz, A. Csík, Z. Kormány, Z. Perduk, F. Kocsis, and I. Rajta, Eur. Phys. J. Plus **136**, 247 (2021).

[19] Z. Korkulu, N. Özkan, G. G. Kiss, T. Szücs, G. Gyürky, Z. Fülöp, R. T. Güray, Z. Halász, T. Rauscher, E. Somorjai, Z. Török, and C. Yalçın, Phys. Rev. C **97**, 045803 (2018).

[20] G. Gyürky, Z. Halász, G. G. Kiss, T. Szücs, R. Huszánk, Z. Török, Z. Fülöp, T. Rauscher, and C. Travaglio, J. Phys. G: Nucl. Part. Phys. **48**, 105202 (2021).

[21] T. Szücs, G. Kiss, T. Rauscher, Z. Töök, Z. Halász, Z. Fülöp, G. Gyürky, and E. Somorjai, J. Phys.: Conf. Ser. **665**, 012041 (2016).

[22] P. Mohr, T. Rauscher, H. Oberhummer, Z. Máté, Z. Fülöp, E. Somorjai, M. Jaeger, and G. Staudt, Phys. Rev. C **55**, 1523 (1997).

[23] A. J. Koning, S. Hilaire, and S. Goriely, computer code TALYS, version 1.9.

[24] P. Mohr, Z. Fülöp, G. Gyürky, G. G. Kiss, and T. Szücs, Phys. Rev. Lett. **124**, 252701 (2020).

[25] P. Mohr, Z. Fülöp, G. Gyürky, G. Kiss, T. Szücs, A. Arcones, M. Jacobi, and A. Psaltis, At. Data Nucl. Data Tables **142**, 101453 (2021).

[26] V. Avrigeanu, M. Avrigeanu, and C. Mănăilescu, Phys. Rev. C **90**, 044612 (2014).

[27] L. McFadden and G. R. Satchler, Nucl. Phys. **84**, 177 (1966).

[28] P. Demetriou, C. Grama, and S. Goriely, Nucl. Phys. A **707**, 253 (2002).

[29] P. Mohr, R. Talwar, and M. L. Avila, Phys. Rev. C **98**, 045805 (2018).

[30] P. Mohr, G. Gyürky, and Z. Fülöp, Phys. Rev. C **95**, 015807 (2017).

[31] S. Watanabe, Nucl. Phys. **8**, 484 (1958).

[32] M. Nolte, H. Machner, and J. Bojowald, Phys. Rev. C **36**, 1312 (1987).

[33] V. Avrigeanu, P. E. Hodgson, and M. Avrigeanu, Phys. Rev. C **49**, 2136 (1994).

[34] T. Rauscher and F.-K. Thielemann, At. Data Nucl. Data Tables **75**, 1 (2000).

[35] R. H. Cyburt, A. M. Amthor, R. Ferguson, Z. Meisel, K. Smith, S. Warren, A. Heger, R. D. Hoffman, T. Rauscher, A. Sakharuk, H. Schatz, F. K. Thielemann, and M. Wiescher, Astrophys. J. Suppl. Ser. **189**, 240 (2010).

[36] P. Mohr, Eur. Phys. J. A **51**, 56 (2015).

[37] A. Sauerwein, H.-W. Becker, H. Dombrowski, M. Elvers, J. Endres, U. Giesen, J. Hasper, A. Hennig, L. Netterdon, T. Rauscher, D. Rogalla, K. O. Zell, and A. Zilges, Phys. Rev. C **84**, 045808 (2011).

[38] P. Mohr, Phys. Rev. C **84**, 055803 (2011).

[39] A. L. Sallaska, C. Iliadis, A. E. Champagne, S. Goriely, S. Starrfield, and F. X. Timmes, Astrophys, J. Suppl. Ser. **207**, 18 (2013).

[40] M. Avrigeanu, W. von Oertzen, A. Plompen, and V. Avrigeanu, Nucl. Phys. A **723**, 104 (2003).

[41] P. Mohr, G. Kiss, Z. Fülöp, D. Galaviz, G. Gyürky, and E. Somorjai, At. Data Nucl. Data Tables **99**, 651 (2013).

[42] L. Fang, P. Frossard, M. Boyet, A. Bouvier, J.-A. Barrat, M. Chaussidon, and F. Moynier, Proc. Natl. Acad. Sci. USA **119**, e2120933119 (2022).

[43] M. Lugaro, M. Pignatari, U. Ott, K. Zuber, C. Travaglio, G. Gyürky, and Z. Fülöp, Proc. Natl. Acad. Sci. USA **113**, 907 (2016).

[44] T. Rauscher, Phys. Rev. Lett. **111**, 061104 (2013).

[45] N. Kinoshita, M. Paul, Y. Kashiv, P. Collon, C. M. Deibel, B. DiGiovine, J. P. Greene, D. J. Henderson, C. L. Jiang, S. T. Marley, T. Nakanishi, R. C. Pardo, K. E. Rehm, D. Robertson, R. Scott, C. Schmitt, X. D. Tang, R. Vondrasek, and A. Yokoyama, Science **335**, 1614 (2012).

[46] A. Gannoun, M. Boyet, H. Rizo, and A. E. Goresy, Proc. Natl. Acad. Sci. USA **108**, 7693 (2011).

[47] S. E. Woosley and W. M. Howard, Astrophys. J. Suppl. Series **36**, 285 (1978).

[48] J. Audouze and D. M. Schramm, Nature (London) **237**, 447 (1972).

[49] A. Prinzhofer, D. A. Papanastassiou, and G. J. Wasserburg, Astrophys. J. **344**, L81 (1989).

[50] A. Prinzhofer, D. Papanastassiou, and G. Wasserburg, Geochim. Cosmochim. Acta **56**, 797 (1992).

[51] L. E. Nyquist, B. Bansal, H. Wiesmann, and C.-Y. Shih, Meteoritics **29**, 872 (1994).

[52] K. Rankenburg, A. D. Brandon, and C. R. Neal, Science **312**, 1369 (2006).

[53] T. Rauscher and F.-K. Thielemann, computer code NON-SMOKER.

[54] T. Rauscher, N. Nishimura, R. Hirschi, G. Cescutti, A. S. J. Murphy, and A. Heger, Mon. Not. R. Astron. Soc. **463**, 4153 (2016).

[55] T. Rauscher, Phys. Rev. C **81**, 045807 (2010).

[56] A. Psaltis, A. Arcones, F. Montes, P. Mohr, C. J. Hansen, M. Jacobi, and H. Schatz, Astrophys. J. **935**, 27 (2022).